

Quantum Properties of Dichroic Silicon Vacancies in Silicon Carbide

Roland Nagy,^{1,†} Matthias Widmann,^{1,†} Matthias Niethammer,¹ Durga B. R. Dasari,¹ Ilja Gerhardt,^{1,2} Öney O. Soykal,³ Marina Radulaski,⁴ Takeshi Ohshima,⁵ Jelena Vučković,⁴ Nguyen Tien Son,⁶ Ivan G. Ivanov,⁶ Sophia E. Economou,⁷ Cristian Bonato,⁸ Sang-Yun Lee,^{9,*} and Jörg Wrachtrup^{1,2}

¹*Third Institute of Physics, University of Stuttgart and Center for Integrated Quantum Science and Technology, IQST, Pfaffenwaldring 57, D-70569 Stuttgart, Germany*

²*Max Planck Institute for Solid State Research, Heisenbergstrasse 1, D-70569 Stuttgart, Germany*

³*Naval Research Laboratory, Washington, D.C. 20375, USA*

⁴*E. L. Ginzton Laboratory, Stanford University, Stanford, California 94305, USA*


⁵*National Institutes for Quantum and Radiological Science and Technology, Takasaki, Gunma 370-1292, Japan*

⁶*Department of Physics, Chemistry, and Biology, Linköping University, SE-58183 Linköping, Sweden*

⁷*Department of Physics, Virginia Polytechnic Institute & State University, Blacksburg, Virginia 24061, USA*

⁸*Institute of Photonics and Quantum Sciences, SUPA, Heriot-Watt University, Edinburgh EH14 4AS, United Kingdom*

⁹*Center for Quantum Information, Korea Institute of Science and Technology, Seoul 02792, Republic of Korea*

 (Received 16 August 2017; revised manuscript received 1 January 2018; published 23 March 2018)

Although various defect centers have displayed promise as either quantum sensors, single photon emitters, or light-matter interfaces, the search for an ideal defect with multifunctional ability remains open. In this spirit, we study the dichroic silicon vacancies in silicon carbide that feature two well-distinguishable zero-phonon lines and analyze the quantum properties in their optical emission and spin control. We demonstrate that this center combines 40% optical emission into the zero-phonon lines showing the contrasting difference in optical properties with varying temperature and polarization, and a 100% increase in the fluorescence intensity upon the spin resonance, and long spin coherence time of their spin-3/2 ground states up to 0.6 ms. These results single out this defect center as a promising system for spin-based quantum technologies.

DOI: [10.1103/PhysRevApplied.9.034022](https://doi.org/10.1103/PhysRevApplied.9.034022)

I. INTRODUCTION

Quantum technologies based on solid-state devices can take advantage of well-established fabrication and control methods developed over the past century. Among several quantum systems, color centers in diamond [1–3] have gained prominence as quantum-enhanced nanoscale sensors [4], coherent spin-photon and spin-phonon interfaces [5–7] and quantum registers [8]. Despite their success, the limited emission rate of indistinguishable photons of, e.g., the nitrogen-vacancy (N-V) center and the difficulties of diamond nanofabrication currently inhibit the progress towards efficient and scalable spin-photon interfacing devices [9] which is a prerequisite for building quantum networks and network-based quantum computing devices. Defect spins in silicon carbide (SiC) have been studied as an analog to diamond color centers, due to their promising complementary properties and the established technologies in growth, doping, and device fabrication [10]. As in diamond, defect

spins in SiC exhibit long coherence times [11–13] and optically detectable spin signals at room temperatures [14–16], down to the individual spin level [17,18]. SiC hosts several defects with addressable electronic spins, including silicon vacancies [13,18], divacancies [12,17], and transition metal impurities [19,20].

II. DICHROIC SILICON VACANCY

The silicon vacancy (V_{Si}) in SiC is one of the naturally occurring point defects [21] and can be created by kicking out silicon atoms using accelerated particles [14]. There have been two competing models for their atomic structure, an isolated negatively charged V_{Si}^- [21,22] and a V_{Si} bonded to a neutral carbon vacancy [16,23], for the precise identity of V_{Si} . While most defects in semiconductors used in quantum technology host a $S = 1/2$ or 1 electronic spin [3,20,22,24], the silicon vacancy (V_{Si}) in hexagonal SiC features a $S = 3/2$ electronic spin in uniaxial crystal lattices. Its ground state was assigned as $S = 1$ [14] but identified as $S = 3/2$ by much experimental evidence [23,25–27]. According to Kramers' theorem [28], the

* sangyun.lee@kist.re.kr

† These authors contributed equally to this work.

degeneracy of a half-integer spin system can only be broken by magnetic fields, making it insensitive to fluctuations in strain, temperature, and electric field. Furthermore, the same Landé g factor of ground and excited states makes the optical transitions corresponding to different spin states spectrally indistinguishable, for any applied magnetic field [21]. These factors have led to a theoretical proposal, by Soykal *et al.* [29,30], of a robust interface between spin and photon polarization, which is not perturbed by environmental noise. Additionally, while other defects exist in several different orientations in the crystal lattice [31,32], V_{Si} at each inequivalent lattice exhibit only one single spin orientation along the c axis of the crystal [14,16]. This can allow deterministic orientation, enhancing scalability in devices. In this work, we demonstrate that the $V1$ center, one of the two V_{Si} centers residing at two inequivalent lattice sites of in $4H$ -SiC [21], features a large fraction of radiation into the zero-phonon lines (ZPL) of up to 40%. In addition, two sharp ZPLs exhibit contrasting polarization properties which may provide an alternate way for quantum control. To discriminate the $V1$ center with the $V2$ center whose ZPL is known to be monochromatic, we call it ‘‘dichroic silicon vacancy’’ through this report. These properties can form the basis of the robust spin-photon interface [29]. We also demonstrate efficient spin polarization and readout resulting in nearly a 100% relative increase in optically detected spin signal allowing the high-fidelity spin-state readout, and long spin coherence time into the millisecond range. We conclude with some considerations about the prospects to realize a robust spin-photon interface [29,30]. While the $V2$ center has been intensively studied in the context of quantum applications [13,18,23,27,33–35], there are only a small number of prior studies for the $V1$ center, mostly due to the absence of spin resonance signals at the elevated temperatures [14,21,33].

III. MATERIALS AND METHODS

All measurements are performed on a commercially available high-purity $4H$ -SiC substrate. The sample is electron irradiated (2 MeV) with a dose of 5×10^{17} electrons/cm² to create a high density of V_{Si} defect centers. The sample is placed in a closed-cycle cryostat from Montana instruments, at a temperature around 5 K. A static magnetic field $B_0 = 60$ and $B_0 = 1000$ G is applied parallel to the c axis by a permanent magnet. Optical excitation is performed either resonantly, by a 858/861-nm laser diode using a Littrow external cavity or off resonantly by a 730-nm laser diode. The light is focused on the sample by a high-NA (0.9) air objective. The rf/MW fields are created by a vector signal generator (Rhode & Schwartz SMIQ 06B), amplified by a 30-W amplifier (Mini-Circuits, LZY – 22+). Radio-frequency (rf) fields are delivered by a copper wire with a diameter of 20 μm , which is spanned on the sample surface. Further information can be found in the Supplemental Material [36].

IV. FLUORESCENCE PROPERTIES

The theoretical energy-level scheme, proposed by the group-theoretical analysis, is sketched in Fig. 1(a). The ground state of $V1$ is a spin quartet of symmetry 4A_2 ($a_1^2 a_1^1 e^2$) and total spin $S = 3/2$ [21]. The ground $|\pm 1/2\rangle$ and $|\pm 3/2\rangle$ sublevels of $V1$ are split by a zero-field splitting (ZFS) of 4 MHz [21]. Two excited states 4E ($a_1^1 a_1^1 e^3$) and 4A_2 ($a_1^2 a_1^1 e^2$) can be selectively excited from the ground state via resonant laser excitation with 1.445 eV (858 nm) and 1.440 eV (861 nm), known as $V1'$ and $V1$ ZPLs, respectively [21,37]. At a temperature of 5.5 K, both the emission of the $V1$ -ZPL transition (4A_2 to 4A_2) and $V1'$ ZPL emission (4E to 4A_2) are observable as shown in Fig. 1(b) and their decay times, the excited state lifetimes, are approximately 6 ns [36]. Their intensities show temperature dependence, i.e., $V1'$ ZPL intensity peaks at around 70 K [Fig. 1(b)]. The energy difference between the ZPLs of $V1$ and $V1'$ is about 4.4 meV, which corresponds to a thermodynamic equivalent temperature of 51 K. The enhanced emission from the $V1'$ transition at elevated temperatures may be understood as a phonon-assisted process [36].

The protocol by Soykal *et al.* for a robust spin-photon interface features the energetically degenerate but orthogonally polarized photons [29,30] associated to $V1$. Here, we report a complete characterization of the polarization properties of $V1'$ and $V1$ ZPL. While some polarization studies are reported in the literature [21,38], we will show that the current model for this defect requires revision.

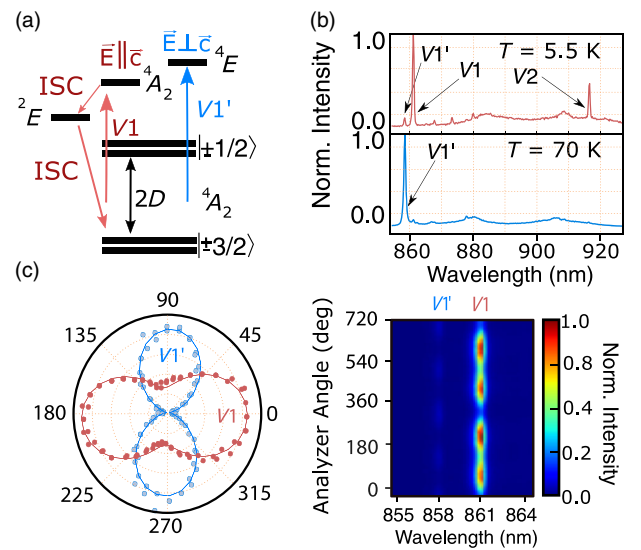


FIG. 1. (a) The energy-level scheme of the $V1$ center. (b) The PL spectrum of a V_{Si} ensemble at 5.5 and 70 K. (c) The optical polarization in which the c axis is perpendicular to the laser incident direction at 5.5 K. Left: the polar plot of the normalized $V1$ and $V1'$ intensities. 0° , equivalently 180° , corresponds to the c -axis orientation. Right: the density plot showing the absolute intensities of the $V1$ - $V1'$ ZPLs.

The polar plot in Fig. 1(c) represents the integrated intensity of each of the $V1$ and $V1'$ ZPLs as a function of the half-wave plate angle, taken at $T = 5.5$ K with the laser incident angle perpendicular to the c axis. The dominant polarizations of $V1$ and $V1'$ ZPLs are almost orthogonal to each other. The full orientation analysis results are in qualitative agreement with previously suggested optical selection rules based on group-theoretical analysis within the single group C_{3v} , representing the symmetry of V_{Si} [21,38]. This analysis predicts $\mathbf{E}\parallel\mathbf{c}$ polarization for the $V1$ transition and $\mathbf{E}\perp\mathbf{c}$ polarization for the $V1'$ transition. However, while the photons originating from $V1'$ are quite well linearly polarized $\mathbf{E}\perp\mathbf{c}$, the $V1$ transition is not entirely polarized as $\mathbf{E}\parallel\mathbf{c}$ but contains a component $\mathbf{E}\perp\mathbf{c}$. These indicate that the selection rules need revision. Since the negatively charged V_{Si} contains an odd number of electrons (resulting in half-integer spin), the correct symmetry is the double-group \overline{C}_{3v} , as previously suggested [29]. The derivation of the selection rules for \overline{C}_{3v} leads to a better estimate of the relative contribution of the $\mathbf{E}\parallel\mathbf{c}$ and $\mathbf{E}\perp\mathbf{c}$ polarizations in the optical emission of the $V1$ and $V1'$ ZPLs. This is outlined in the Supplemental Material [36]. We find that for the $V1$ transition the distribution among the two polarizations is $\mathbf{E}\parallel\mathbf{c}:\mathbf{E}\perp\mathbf{c} = 3:1$, whereas for the $V1'$ transition the proportion is $\mathbf{E}\perp\mathbf{c}:\mathbf{E}\parallel\mathbf{c} = 11:1$. These estimates are in good agreement with the polar plots in Fig. 1(c), $\mathbf{E}\parallel\mathbf{c}/\mathbf{E}\perp\mathbf{c} = 1.85 \pm 0.06$ for $V1$, and $\mathbf{E}\perp\mathbf{c}/\mathbf{E}\parallel\mathbf{c} = 19 \pm 3$ for $V1'$. For completeness, polarization is also measured with the laser incident angle parallel to the c axis [36].

V. OPTICAL SPIN-STATE DETECTION

In the next set of measurements, we characterize the spin properties for a defect ensemble. The ground-state spin can be polarized into the sublevels $|S_z = \pm 3/2\rangle$ [29] by optical pumping [33] with an off-resonant laser ($\lambda = 730$ nm). At any constant finite magnetic fields (B_0), the spin energy levels are determined by the Hamiltonian,

$$H = g\mu_B\mathbf{B}\cdot\mathbf{S} + D[S_Z^2 - S(S+1)/3], \quad (1)$$

where g is the Landé g factor, μ_B is the Bohr magneton, D is the ZFS ($2D = 4$ MHz), and S_Z is the projection of the total spin onto the quantization axis, the c axis in $4H$ -SiC. By applying resonant rf fields (B_1) one can induce transitions between spin sublevels [Fig. 2(a)], resulting in a change in optically detected magnetic resonance (ODMR) as shown in Fig. 2(b). The relative change in ODMR signal is calculated as $[I(f) - I_{\text{off}}]/I_{\text{off}}$, where $I(f)$ is the PL intensity at the rf frequency f , and I_{off} is the PL intensity at the off-resonant rf frequency. The spin sublevels are energetically split at $B_0 = 60$ G aligned along the c axis. The relative ODMR signal as a function of the driving rf frequency shows a negative signal at 170 MHz, with the relative intensity 0.05% as in the upper panel of Fig. 2(b). It is attributed to the $V1$ ground-state spin; a similar signal

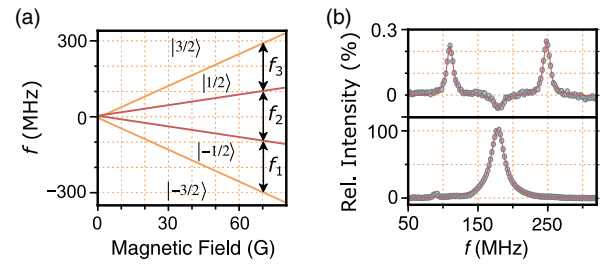


FIG. 2. (a) Zeeman effect of the spin 3/2 ground state of the $V1$ center for $B_0\parallel c$. f_1 , f_2 , and f_3 represent possible resonant transitions. (b) Upper panel: an ensemble ODMR spectrum with a 730-nm laser at 60 G. Two peaks at around 110 and 250 MHz are from the $V2$ center. Lower panel: the ODMR with a laser resonant to $V1$, 861 nm.

is also reported for $V1$ and $V3$ centers in $6H$ -SiC [33]. By exciting the optical transition $V1$ resonantly as in Fig. 1(a) a positive relative ODMR signal with $100 \pm 0.6\%$ is achieved [lower panel in Fig. 2(b)]. In contrast, excitation of the $V1'$ optical transition reveals a negative signal with a minimal change in the relative signal intensity [36]. A similar substantial enhancement of the ODMR signal is reported for the $V2$ center ensemble in $6H$ -SiC [33]. Although the underlying mechanism is not yet completely understood, we attribute it to the enhanced spin polarization in the ground state resulting from resonant optical excitation. Resonant excitation of $V1$ ZPL results in the excitation into the lowest vibrational level of the $V1$ excited state. This efficiently suppresses the phonon-assisted spin mixing between the 4A_2 and 4E excited states leading to an improvement in the ODMR signal at sufficiently low temperatures ($k_B T < 4.4$ meV). On the other hand, resonant excitation of $V1'$ does not result in such an improvement, as it still involves the excitation of $V1$ (lower in energy) and its vibrational levels. This observation may also indicate that optical polarization is mainly established by the intersystem crossing (ISC) between the 4A_2 excited states and the 2E metastable state while the 4E excited states have a less-efficient ISC [29]. We expect further enhancement of the ODMR signal when a single $V1$ center is isolated owing to the suppressed inhomogeneous broadening. We note that if an identical ODMR contrast, namely C , and an identical photoluminescence (PL) intensity without spin resonance are assumed, a positive signal leads to a signal-to-noise ratio larger than the negative signal, as of the N-V center in diamond [1] and divacancies in $4H$ - and $6H$ -SiC [32], by a factor of $(1 - C)^{-0.5}$ [36].

VI. COHERENT SPIN CONTROL

In order to demonstrate coherent control of the electronic spins, we investigate spin dynamics of the $V1$ center ensemble under applied rf pulses. The resulting distribution of the Rabi oscillations in the range of $f = 160$ – 190 MHz at $B_0 = 60$ G is shown in Fig. 3(a). The dynamics is

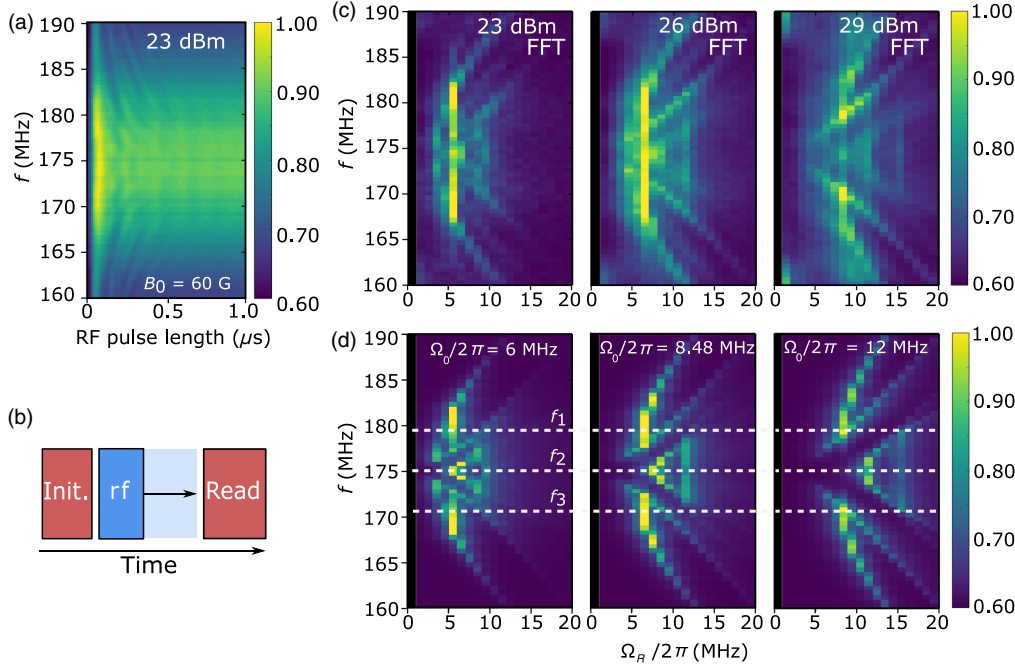


FIG. 3. (a) Rabi measurement with detuned rf driving frequencies. (b) Pulse scheme for a Rabi measurement. The first laser pulse (Init.) polarizes the spin state. The rf pulse manipulates the spin state followed by the last laser pulse (Read) for the spin-state readout. (c) Fast-Fourier-transformed Rabi oscillations at different rf powers. (d) Simulated Rabi oscillations. The dotted lines indicate three resonant rf frequencies shown in Fig. 2(a). The strong zero-frequency intensities in both (c) and (d) are removed for better distinguishability of the Rabi frequencies.

strikingly different from the single-frequency Rabi oscillations typical of a two-level system. Further understanding can be obtained by plotting the fast-Fourier transform of the Rabi oscillations, for different values of the driving power. For two-level transitions one expects parabolic profiles, corresponding to a Rabi frequency Ω increasing with the detuning $\Delta\omega$ as $\Omega^2 = \Omega_0^2 + \Delta\omega^2$ where Ω_0 is the driving frequency determined by the applied B_1 field strength ($\Omega_0 \propto B_1$). The experimental data reveal richer and more complex dynamics. We explain our observations with the presence of three closely spaced transitions, corresponding to f_1 , f_2 , and f_3 in Fig. 2(a). While resonantly driving one transition, due to the small ZFS, off-resonant excitation of the other two transitions is not negligible. To support this explanation, we develop a theoretical model based on four levels of $S = 3/2$ driven by a single monochromatic radio-frequency field. The system dynamics is investigated assuming initial polarization into an incoherent mixture of $|S_z = \pm 3/2\rangle$. Further details on the model can be found in the Supplemental Material [36]. Our simulations match quite closely the complex structure of the experimental data [see Figs. 3(c) and 3(d)]. When f is lower than f_1 ($|-3/2\rangle \leftrightarrow |-1/2\rangle$), the transition f_1 is mainly excited, leading to a parabolic profile. However, off-resonant excitation of the transition f_2 , coupling $|-1/2\rangle$ to $|+1/2\rangle$, results in a second weaker Fourier component in the Rabi spectrum with larger Rabi frequency. With increasing rf power (B_1 field strength), simulated by increasing the driving frequency proportional to the increase of the experimentally used B_1 field strength, this component becomes stronger. When $f = f_2$, one simultaneously drives off resonantly the transitions f_1 and f_3 , resulting in a larger Rabi frequency. This is evident in the plots corresponding to the largest rf power,

where the parabolic profile centered around f_2 shows a much larger Rabi frequency than the profiles related to f_1 and f_3 . Note that the experimental data can only be explained by assuming the excitation of the $|-1/2\rangle \leftrightarrow |+1/2\rangle$ transition, which is not reported. Additionally, the assumption for initial polarization into $|\pm 1/2\rangle$, which is the case for the V2 center, does not reproduce the observed signal. Note that we report the experimental evidence for $S = 3/2$ of the ground state of the V1 in 4H-SiC [36].

The small ZFS poses challenges for high-fidelity coherent spin control, which need to be addressed for the V1 center to be a serious contender for quantum technology. There are several possibilities to explore: the use of (i) optimal quantum control sequences, (ii) adiabatic passage techniques that restrict the dynamics only to a two-level subspace (e.g., $|+3/2\rangle$ and $|-1/2\rangle$), with no leakage to other states of the Hilbert space [39], (iii) pulses designed to avoid a transition by building holes in their frequency spectrum to avoid leakage [40], (iv) superadiabatic (shortcuts to adiabaticity) control [41], which was recently demonstrated for N-V centers in diamond [42]. Alternatively, the V1 in 6H-SiC is known to exhibit a larger ZFS [14,21], which would relax this problem.

VII. SPIN DECOHERENCE

We study spin coherence at $T = 5.5$ K with $B_0 = 60$ G [36] and 1000 G by Ramsey, Hahn-echo, and XY-8 dynamical decoupling pulse sequences by optical excitation resonant with the V1 ZPL (861 nm). We observe an evolution of the coherent superposition with the electron spin dephasing time of $T_2^* = 1.3 \pm 0.3 \mu\text{s}$ at $B_0 = 1000$ G aligned parallel to the c axis by a Ramsey experiment, as

shown in Fig. 4(a). To suppress the inhomogeneous broadening in an ensemble and decouple the spin ensembles from low-frequency spin noise from such as paramagnetic impurities and a nuclear spin bath composed of ^{29}Si and ^{13}C [11], we apply a Hahn-Echo sequence. Identical laser pulses of $2\text{-}\mu\text{s}$ length are applied before and after the MW pulse sequences for the optical spin polarization and projective spin-state readout, respectively, and also to avoid dephasing due to the optical excitation [29]. Although the applied rf pulses exhibit limited spin control to a single transition as discussed in the Supplemental Material [36], we can see a typical exponential decay with $T_2 = 83.9 \pm 1.6 \mu\text{s}$ [Fig. 4(b)]. The observed T_2 is, however, shorter than the theoretical expectations for the V_2 center [11] and the value measured for a single V_2 center at room temperature [18]. This could be related to the imperfect π pulses and the inhomogeneity of the B_0 field (see the Supplemental Material [36]). These observations, however, support the findings by Carter *et al.* [34], related to the fact that the dephased state cannot be refocused by a π pulse due to the oscillating local fields produced by coupled nuclear spins. Thus, the shorter T_2 could be related to electron spin echo envelope modulation (ESEEM). The four sublevels of a $S = 3/2$ electronic spin have four different nonzero hyperfine couplings to nearby nuclear spins and thus result in more complex ESEEM than $S = 1$ systems [11,18]. Furthermore, as reported by Carter *et al.*, the ensemble inhomogeneous broadening induces beating oscillations among the various modulation frequencies, leading to a shortening of the Hahn-echo T_2 [34]. To further suppress decoherence, we apply the XY-8 dynamical decoupling sequence, which acts as a filter for the environmental magnetic noise [43]. This sequence has proven to be effective in extending the coherence time of the $S = 3/2$ spin ensemble of the V_2 center from the nuclear spin bath in $4H\text{-SiC}$ [13]. A repeated decoupling pulse scheme leads to a better suppression of noise, increasing the spin decoherence time with $N = 10$ and $N = 50$ repetitions to a value of, respectively, $T_2 = 286 \pm 7 \mu\text{s}$ and $T_2 = 0.60 \pm 0.01 \text{ ms}$ [Fig. 4(b)]. These suggest that the heteronuclear spin bath in SiC itself provides a diluted spin bath for not

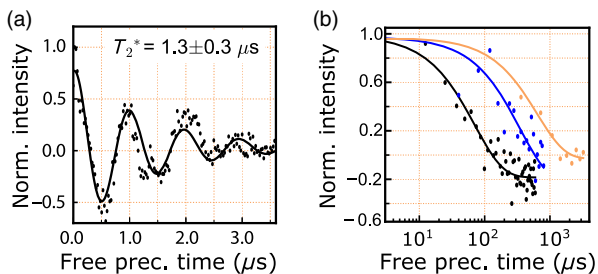


FIG. 4. (a) Ramsey measurement at $B_0 = 1000 \text{ G}$. (b) The spin decoherence measured at $B_0 = 1000 \text{ G}$ by Hahn-Echo (black) and XY-8 dynamic decoupling (blue, $N = 10$; orange, $N = 50$). See the Supplemental Material for the used pulse sequence [36].

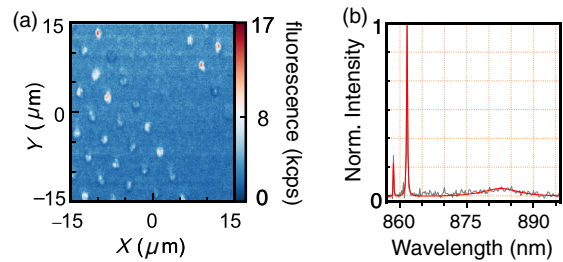


FIG. 5. (a) Confocal fluorescence raster scan showing single silicon vacancy V_1 and V_2 centers in SiC nanopillars at 4 K . (b) A single V_1 defect PL spectrum with the V_1' and V_1 ZPLs at 858 and 861 nm , respectively.

only the V_2 center [13,18], and divacancy defects [17], but also the V_1 center.

VIII. ISOLATED SINGLE SILICON VACANCY

Although the spin-ensemble-based quantum applications such as quantum memory [44] are valuable, many advanced quantum applications including, e.g., the spin-photon interface requires addressing of single defect centers. To test if the single V_1 center can be used as an efficient coherent single photon source, e.g., a building block for the robust spin-photon interface, we isolate single V_1 centers in nanopillars fabricated on a $4H\text{-SiC}$ sample [35], as shown in Fig. 5(a). Addressing of a single center is proven by the autocorrelation measurement in a Hanbury, Brown, and Twiss configuration, with $g^{(2)} < 0.5$ [36]. The saturated count rate of 14 kcps is measured by an air objective of $\text{NA} = 0.9$ with a single photon detector inefficient in this wavelength (see the Supplemental Material [36]). The spectrum at $T = 4 \text{ K}$ shows both V_1 and V_1' ZPLs as in Fig. 5(b), further proof that they correspond to two different excited states of the same defect. To determine the Debye-Waller factor (DWF), the fraction of radiation into the ZPL of V_1 over the whole V_1 spectrum, the contribution of V_1' to the phonon sideband (PSB) has to be minimized. At 4 K , the intensity of the V_1' ZPL is weak, and we suppose that the contribution to the PSB is also negligible in comparison to V_1 . Then, the conservatively estimated DWF of the V_1 is $40 \pm 6\%$. See the Supplemental Material [36] for the additional data and DWF of the V_1' .

IX. SUMMARY AND OUTLOOK

In summary, optical spectroscopy and polarization measurements confirm the symmetry properties of the V_1 center in $4H\text{-SiC}$, supported by the established double-group \overline{C}_{3v} model, substantiating the theoretical model leading to the proposed robust spin-photon interface [29]. A spin-photon interface requires narrow optical transitions [36], weak spectral diffusion, and slow spin-flip rates by optical pumping cycles. Recent results on the divacancy in SiC show that the material quality is

sufficiently high to satisfy these requirements [22]. Resonant optical excitation of the $V1$ ZPL leads to a substantial increase in spin-dependent photoluminescence emission, indicating an efficient spin-dependent transition. We also show the extension of spin coherence time, through dynamical decoupling sequences, up to 0.6 ms, which will enable long and complex spin manipulation necessary for the spin-photon interface [5,45]. While the leading contenders for defect-based quantum spintronics, such as the N-V center in diamond and divacancy in 4H-SiC, suffer from low optical emission into zero-phonon lines (with DWF $\sim 3\%$ and $5\%–7\%$ [22,46], respectively), the $V1$ center in 4H-SiC features a significantly higher DWF, up to 40%. The high ZPL emission could guarantee a high event rate for the proposed generation of spin-photon entanglement. The weak overall photon emission rate of the $V1$ and $V1'$ transition may be circumvented by using photonic structures fabricated on SiC, which recently have shown progress towards high- Q cavities and efficient photon collection [35,37,47]. This can further be used to generate strings of entangled photons [6,48]. Further work on this dichroic single defect, which is ongoing, is necessary to identify individual optical transitions and the associated selection rules which are essential for realizing spin-photon interfaces, e.g., spin-photon entanglement exploiting transitions to the 4E excited state ($V1'$ line) with the high-fidelity spin initialization and readout with the $V1$ line.

ACKNOWLEDGMENTS

This work was supported by the ERA.Net RUS Plus Program (DIABASE), the DFG via priority programme 1601, the EU via ERC Grant SMel and Diadems, the Max Planck Society, the Carl Zeiss Stiftung, the Swedish Research Council (VR 2016-04068), the Carl-Trygger Stiftelse för Vetenskaplig Forskning (CTS 15:339), the Knut and Alice Wallenberg Foundation (KAW 2013.0300), the JSPS KAKENHI (A) 17H01056, the National Science Foundation DMR Grant No. 1406028, the U.S. Office of Secretary of Defense Quantum Science and Engineering Program, the COST Action MP1403 “Nanoscale Quantum Optics” funded by COST (European Cooperation in Science and Technology), and by EPSRC (Grant No. EP/P019803/1), the Army Research Office under Contract No. W911NF1310309, and the KIST Open Research Program (2E27231) and institutional program (2E27110). We thank Roman Kolesov, Rainer Stöhr, and Torsten Rendler for fruitful discussions and experimental aid. We also acknowledge motivating discussions with Michel Bockstedte, Adam Gali, Thomas L. Reinecke, and Jingyuan Linda Zhang.

[1] G. Balasubramanian, P. Neumann, D. Twitchen, M. Markham, R. Kolesov, N. Mizuochi, J. Isoya, J. Achard,

- J. Beck, J. Tessler, V. Jacques, P. R. Hemmer, F. Jelezko, and J. Wrachtrup, Ultralong spin coherence time in isotopically engineered diamond, *Nat. Mater.* **8**, 383 (2009).
- [2] T. Häberle, D. Schmid-Lorch, K. Karrai, F. Reinhard, and J. Wrachtrup, High-Dynamic-Range Imaging of Nanoscale Magnetic Fields Using Optimal Control of a Single Qubit, *Phys. Rev. Lett.* **111**, 170801 (2013).
- [3] D. D. Awschalom, L. C. Bassett, A. S. Dzurak, E. L. Hu, and J. R. Petta, Quantum spintronics: Engineering and manipulating atom-like spins in semiconductors, *Science* **339**, 1174 (2013).
- [4] N. Aslam, M. Pfender, P. Neumann, R. Reuter, A. Zappe, F. Fávoro de Oliveira, A. Denisenko, H. Sumiya, S. Onoda, J. Isoya, and J. Wrachtrup, Nanoscale nuclear magnetic resonance with chemical resolution, *Science* **357**, 67 (2017).
- [5] S. Yang, Y. Wang, D. D. B. Rao, T. Hien Tran, A. S. Momenzadeh, M. Markham, D. J. Twitchen, P. Wang, W. Yang, R. Stöhr, P. Neumann, H. Kosaka, and J. Wrachtrup, High-fidelity transfer and storage of photon states in a single nuclear spin, *Nat. Photonics* **10**, 507 (2016).
- [6] D. D. B. Rao, S. Yang, and J. Wrachtrup, Generation of entangled photon strings using NV centers in diamond, *Phys. Rev. B* **92**, 081301 (2015).
- [7] D. A. Golter, T. Oo, M. Amezcua, K. A. Stewart, and H. Wang, Optomechanical Quantum Control of a Nitrogen-Vacancy Center in Diamond, *Phys. Rev. Lett.* **116**, 143602 (2016).
- [8] G. Waldherr, Y. Wang, S. Zaiser, M. Jamali, T. Schulte-Herbrüggen, H. Abe, T. Ohshima, J. Isoya, J. F. Du, P. Neumann, and J. Wrachtrup, Quantum error correction in a solid-state hybrid spin register, *Nature (London)* **506**, 204 (2014).
- [9] L. Li, T. Schröder, E. H. Chen, M. Walsh, I. Bayn, J. Goldstein, O. Gaathon, M. E. Trusheim, M. Lu, J. Mower, M. Cotlet, M. L. Markham, D. J. Twitchen, and D. Englund, Coherent spin control of a nanocavity-enhanced qubit in diamond, *Nat. Commun.* **6**, 6173 (2015).
- [10] T. Kimoto and J. A. Cooper, *Fundamentals of Silicon Carbide Technology: Growth, Characterization, Devices and Applications* (John Wiley & Sons, Singapore, 2014).
- [11] L. P. Yang, C. Burk, M. Widmann, S. -Y. Lee, J. Wrachtrup, and N. Zhao, Electron spin decoherence in silicon carbide nuclear spin bath, *Phys. Rev. B* **90**, 241203 (2014).
- [12] H. Seo, A. L. Falk, P. V. Klimov, K. C. Miao, G. Galli, and D. D. Awschalom, Quantum decoherence dynamics of divacancy spins in silicon carbide, *Nat. Commun.* **7**, 12935 (2016).
- [13] D. Simin, H. Kraus, A. Sperlich, T. Ohshima, G. V. Astakhov, and V. Dyakonov, Locking of electron spin coherence above 20 ms in natural silicon carbide, *Phys. Rev. B* **95**, 161201 (2017).
- [14] E. Sörman, N. Son, W. Chen, O. Kordina, C. Hallin, and E. Janzén, Silicon vacancy related defect in 4H and 6H SiC, *Phys. Rev. B* **61**, 2613 (2000).
- [15] W. F. Koehl, B. B. Buckley, F. J. Heremans, G. Calusine, and D. D. Awschalom, Room temperature coherent control of defect spin qubits in silicon carbide, *Nature (London)* **479**, 84 (2011).
- [16] V. A. Soltamov, B. V. Yavkin, D. O. Tolmachev, R. A. Babunts, A. G. Badalyan, V. Y. Davydov, E. N. Mokhov,

- I. I. Proskuryakov, S. B. Orlinskii, and P. G. Baranov, Optically Addressable Silicon Vacancy-Related Spin Centers in Rhombic Silicon Carbide with High Breakdown Characteristics and ENDOR Evidence of Their Structure, *Phys. Rev. Lett.* **115**, 247602 (2015).
- [17] D. Christle, A. Falk, P. Andrich, P. V. Klimov, J. Ul Hassan, N. T. Son, E. Janzén, T. Ohshima, and D. D. Awschalom, Isolated electron spins in silicon carbide with millisecond-coherence times, *Nat. Mater.* **14**, 160 (2015).
- [18] M. Widmann, S.-Y. Lee, T. Rendler, N. T. Son, H. Fedder, S. Paik, L.-P. Yang, N. Zhao, S. Yang, I. Booker, A. Denisenko, M. Jamali, S. A. Momenzadeh, I. Gerhardt, T. Ohshima, A. Gali, E. Janzén, and J. Wrachtrup, Coherent control of single spins in silicon carbide at room temperature, *Nat. Mater.* **14**, 164 (2015).
- [19] K. Lee, L. Dang, G. Watkins, and W. Choyke, Optically detected magnetic resonance study of SiC:Ti, *Phys. Rev. B* **32**, 2273 (1985).
- [20] W. F. Koehl, B. Diler, S. J. Whiteley, A. Bourassa, N. T. Son, E. Janzén, and D. D. Awschalom, Resonant optical spectroscopy and coherent control of Cr⁴⁺ spin ensembles in SiC and GaN, *Phys. Rev. B* **95**, 035207 (2017).
- [21] E. Janzén, A. Gali, P. Carlsson, A. Gällström, B. Magnusson, and N. T. T. Son, The silicon vacancy in SiC, *Physica (Amsterdam)* **404B**, 4354 (2009).
- [22] D. J. Christle, P. V. Klimov, C. F. Casas, K. Szász, V. Ivády, V. Jokubavicius, M. Syväjärvi, W. F. Koehl, T. Ohshima, and N. T. Son, Isolated Spin Qubits in SiC with a High-Fidelity Infrared Spin-to-Photon Interface, *Phys. Rev. X* **7**, 021046 (2017).
- [23] H. Kraus, V. a. Soltamov, D. Riedel, S. Váth, F. Fuchs, a. Sperlich, P. G. Baranov, V. Dyakonov, and G. V. Astakhov, Room-temperature quantum microwave emitters based on spin defects in silicon carbide, *Nat. Phys.* **10**, 157 (2014).
- [24] M. Veldhorst, C. H. Yang, J. C. C. Hwang, W. Huang, J. P. Dehollain, J. T. Muhonen, S. Simmons, A. Laucht, F. E. Hudson, K. M. Itoh, A. Morello, and A. S. Dzurak, A two-qubit logic gate in silicon, *Nature (London)* **526**, 410 (2015).
- [25] T. Wimbauer, B. K. Meyer, A. Hofstaetter, A. Scharmann, and H. Overhof, Negatively charged Si vacancy in 4H SiC: A comparison between theory and experiment, *Phys. Rev. B* **56**, 7384 (1997).
- [26] N. Mizuochi, S. Yamasaki, H. Takizawa, N. Morishita, T. Ohshima, H. Itoh, and J. Isoya, Continuous-wave and pulsed EPR study of the negatively charged silicon vacancy with $S = 3/2$ and C_{3v} symmetry in N-type 4H-SiC, *Phys. Rev. B* **66**, 235202 (2002).
- [27] M. Niethammer, M. Widmann, S.-Y. Lee, P. Stenberg, O. Kordina, T. Ohshima, N. T. Son, E. Janzén, and J. Wrachtrup, Vector Magnetometry Using Silicon Vacancies in 4H-SiC Under Ambient Conditions, *Phys. Rev. Applied* **6**, 034001 (2016).
- [28] N. M. Atherton, *Principles of Electron Spin Resonance*, Ellis Horwood Series in Physical Chemistry (Ellis Horwood, Hemel Hempstead, U.K., 1993).
- [29] Ö. O. Soykal, P. Dev, and S. E. Economou, Silicon vacancy center in 4H-SiC: Electronic structure and spin-photon interfaces structure and spin-photon interfaces, *Phys. Rev. B* **93**, 081207(R) (2016).
- [30] S. E. Economou and P. Dev, Spin-photon entanglement interfaces in silicon carbide defect centers, *Nanotechnology* **27**, 504001 (2016).
- [31] J. Michl, T. Teraji, S. Zaiser, I. Jakobi, G. Waldherr, F. Dolde, P. Neumann, M. W. Doherty, N. B. Manson, J. Isoya, and J. Wrachtrup, Perfect alignment and preferential orientation of nitrogen-vacancy centers during chemical vapor deposition diamond growth on (111) surfaces, *Appl. Phys. Lett.* **104**, 102407 (2014).
- [32] A. L. Falk, B. B. Buckley, G. Calusine, W. F. Koehl, V. V. Dobrovitski, A. Politi, C. A. Zorman, P. X.-L. Feng, D. D. Awschalom, V. Viatcheslav, A. Politi, C. A. Zorman, X. Feng, and D. D. Awschalom, Polytype control of spin qubits in silicon carbide, *Nat. Commun.* **4**, 1819 (2013).
- [33] P. Baranov, A. Bundakova, A. Soltamova, S. Orlinskii, I. Borovykh, R. Zondervan, R. Verberk, and J. Schmidt, Silicon vacancy in SiC as a promising quantum system for single-defect and single-photon spectroscopy, *Phys. Rev. B* **83**, 125203 (2011).
- [34] S. G. Carter, Ö. O. Soykal, P. Dev, S. E. Economou, and E. R. Glaser, Spin coherence and echo modulation of the silicon vacancy in 4H-SiC at room temperature, *Phys. Rev. B* **92**, 161202 (2015).
- [35] M. Radulaski, M. Widmann, M. Niethammer, J. L. Zhang, S.-Y. Lee, T. Rendler, K. G. Lagoudakis, N. T. Son, E. Janzen, T. Ohshima, J. Wrachtrup, and J. Vučković, Scalable quantum photonics with single color centers in silicon carbide, *Nano Lett.* **17**, 1782 (2017).
- [36] See Supplemental Material at <http://link.aps.org/supplemental/10.1103/PhysRevApplied.9.034022> for further details.
- [37] D. O. Bracher, X. Zhang, and E. L. Hu, Selective Purcell enhancement of two closely linked zero-phonon transitions of a silicon carbide color center, *Proc. Natl. Acad. Sci. U.S.A.* **114**, 4060 (2017).
- [38] M. Wagner, B. Magnusson, W. Chen, E. Janzén, E. Sörman, C. Hallin, and J. Lindström, Electronic structure of the neutral silicon vacancy in 4H and 6H SiC, *Phys. Rev. B* **62**, 16555 (2000).
- [39] J. Oreg, F. T. Hioe, and J. H. Eberly, Adiabatic following in multilevel systems, *Phys. Rev. A* **29**, 690 (1984).
- [40] C. Neill, P. Roushan, M. Fang, Y. Chen, M. Kolodrubetz, Z. Chen, A. Megrant, R. Barends, B. Campbell, B. Chiaro, A. Dunsworth, E. Jeffrey, J. Kelly, J. Mutus, P. J. J. O'Malley, C. Quintana, D. Sank, A. Vainsencher, J. Wenner, T. C. White, A. Polkovnikov, and J. M. Martinis, Ergodic dynamics and thermalization in an isolated quantum system, *Nat. Phys.* **12**, 1037 (2016).
- [41] M. V. Berry, Transitionless quantum driving, *J. Phys. A* **42**, 365303 (2009).
- [42] B. B. Zhou, A. Baksic, H. Ribeiro, C. G. Yale, F. J. Heremans, P. C. Jerger, A. Auer, G. Burkard, A. A. Clerk, and D. D. Awschalom, Accelerated quantum control using superadiabatic dynamics in a solid-state lambda system, *Nat. Phys.* **13**, 330 (2017).
- [43] A. M. Souza, G. A. Álvarez, and D. Suter, Robust dynamical decoupling, *Phil. Trans. R. Soc. A* **370**, 4748 (2012).
- [44] P. V. Klimov, A. L. Falk, D. J. Christle, V. V. Dobrovitski, and D. D. Awschalom, Quantum entanglement at ambient

- conditions in a macroscopic solid-state spin ensemble, *Sci. Adv.* **1**, e1501015 (2015).
- [45] E. Togan, Y. Chu, A. S. Trifonov, L. Jiang, J. Maze, L. Childress, M. V. G. Dutt, A. S. Sørensen, P. R. Hemmer, A. S. Zibrov, and M. D. Lukin, Quantum entanglement between an optical photon and a solid-state spin qubit, *Nature (London)* **466**, 730 (2010).
- [46] A. Alkauskas, B. B. Buckley, D. D. Awschalom, and C. G. Van De Walle, First- principles theory of the luminescence lineshape for the triplet transition in diamond NV centres, *New J. Phys.* **16**, 073026 (2014).
- [47] A. P. Magyar, D. Bracher, J. C. Lee, I. Aharonovich, and E. L. Hu, High quality SiC microdisk resonators fabricated from monolithic epilayer wafers, *Appl. Phys. Lett.* **104**, 051109 (2014).
- [48] N. H. Lindner and T. Rudolph, Proposal for Pulsed On-Demand Sources of Photonic Cluster State Strings, *Phys. Rev. Lett.* **103**, 113602 (2009).